IEEE Access
Multidisciplinary ⋮ Rapid Review ⋮ Open Access Journal

Received February 3, 2021, accepted March 3, 2021, date of publication March 10, 2021, date of current version March 19, 2021.

Digital Object Identifier 10.1109/ACCESS.2021.3065214

Compressive-Sensing-Aided MIMO Radar Enabling Multi-Functional and Compact Sensors in Air Scenarios Using Optimized Antenna Arrays

ANDREJ HARLAKIN[1], JAN MIETZNER[2], (Senior Member, IEEE), PETER ADAM HOEHER[1], (Fellow, IEEE), AND ASKOLD MEUSLING[3]

[1]Chair of Information and Coding Theory, Christian-Albrechts-University of Kiel, 24143 Kiel, Germany
[2]Faculty of Design, Media and Information, Hamburg University of Applied Sciences, 22081 Hamburg, Germany
[3]Airbus Defence and Space GmbH, 82024 Taufkirchen, Germany

Corresponding author: Andrej Harlakin (anha@tf.uni-kiel.de)

ABSTRACT We address the problem of direction-of-arrival (DoA) estimation for air targets using a compact, multi-functional radar sensor. In order to enhance the angular resolution of such sensors while exploiting the sparseness of typical air scenarios, we consider the combination of a multiple-input multiple-output (MIMO) radar approach with suitable compressive-sensing (CS) techniques. In particular, we investigate the combination of MIMO processing for two-dimensional (2D) antenna arrays with CS-based angular processing for three-dimensional (3D) target localization and 2D DoA estimation in azimuth and elevation. We analyze the benefits of randomized antenna element positions in one and two dimensions and devise optimized array geometries for practicable aperture sizes. In particular, we take physical side constraints into account, such as the smallest realizable/ desired element spacing as well as area restrictions for antenna placement within the overall aperture. The aperture area reserved by this means could be used to accommodate additional hardware components enabling a multi-functional sensor approach. Extensive computer simulation results for different 3D target scenarios illustrate the advantages of our CS-based compact MIMO radar approach with randomized antenna elements compared to fully randomized arrays, given the same number of physical antenna elements.

INDEX TERMS Array optimization, compressive sensing, direction-of-arrival (DoA) estimation, multi-functional sensor, multiple-input multiple-output (MIMO) radar, mutual coherence, target object detection.

I. INTRODUCTION

Radar sensors are nowadays employed for various applications – ranging from target detection and measurement instrumentation to remote sensing and high-resolution imaging [1]–[4]. Generally, radars actively emit radio signals and extract information from the environment by analyzing the corresponding received echo signals. Compared to optical cameras, radars are thus independent of external light sources, rendering them suitable for day- and night-time operation under diverse weather conditions. Moreover, range gating allows to discriminate objects in range direction – typically with high resolution. One drawback of radar sensors, however, is their limited resolution capability in cross-range direction, which is determined by the physical size of the antenna aperture and the employed radar wavelength. Fortunately, advanced signal processing techniques – notably synthetic aperture radar (SAR) [5]–[7] and multiple-input multiple-output (MIMO) radar [8] – are able to alleviate this drawback.

MIMO radar employs multiple antenna elements in conjunction with orthogonal transmit signals and performs joint spatial processing of received signals in the digital domain. As a result, it offers various advantages with regard to radar imaging and target detection. MIMO radars with distributed antenna elements were shown to provide improved detection and parameter estimation performance for fluctuating targets by exploiting spatial diversity effects [9]. MIMO radars with co-located antennas, on the other hand, achieve enhanced angular resolutions based on a virtual enlargement of the

The associate editor coordinating the review of this manuscript and approving it for publication was Wei Wang.

physical antenna aperture [8], which is particularly attractive for compact radar sensors [10], [11].

Independently, compressive sensing (CS) [12]–[15] has been identified as a promising signal processing paradigm for radar applications [16], [17] – among various other application areas ranging from medical imaging to digital communications and audio processing, to name a few. The reason is that radar applications are often characterized by sparse scenarios, where few targets are present in range, Doppler or angular domain, embedded in background noise or clutter. CS techniques are then able to detect such sparse targets and provide estimates for corresponding range, velocity, and direction parameters, while requiring a relatively small number of (generalized) samples compared to traditional Nyquist sampling. Correspondingly, the amount of data generated at the receiver side may be vastly reduced to relax demands on memory space and real-time processing.

In this paper, focus is on direction-of-arrival (DoA) estimation for air targets using a compact radar sensor, e.g., for airborne platforms. In particular, compact radar sensors with a two-dimensional (2D) antenna aperture are considered, offering three-dimensional (3D) target localization in range, azimuth and elevation. Such radar sensors are expected to play a key role with regard to mandatory detect-and-avoid solutions for future air traffic scenarios, especially with regard to unmanned aerial vehicles (UAVs). Examples include autonomous flying taxis and larger cargo drones, which are likely to disrupt traditional air traffic operation within upcoming years. In order to enhance the angular resolution of such radar sensors while at the same time exploiting the sparseness of typical air target scenarios, it is therefore very attractive to combine MIMO radar and CS techniques in a suitable fashion. However, such a combination is not straightforward, since MIMO processing at the receiver somewhat compromises CS-aided DoA estimation. The reason is that conventional MIMO processing (e.g., based on co-located linear antenna arrays) generates a virtual antenna array (VAA), which exhibits a highly regular spatial structure, while CS typically relies on a quasi-random sampling process. In the case of CS-aided DoA estimation, irregular antenna arrays are therefore advantageous for sampling in the spatial domain, which contradicts the conventional MIMO paradigm.

CS for DoA estimation was, for example, addressed in [18], [19], where focus was on conventional one-dimensional (1D) antenna arrays (i.e., the aspect of MIMO processing was not addressed). It was noted that for DoA estimation the resulting measurement matrix is tightly linked to the antenna array geometry. It is well known that the measurement matrix in CS should be random-like, in order to attain good performance results. Using a uniform linear antenna array (ULAA), however, the (mutual) coherence of the measurement matrix was found to be generally close to one, which leads to poor detection and DoA estimation performance under CS. In order to mitigate this effect, it was therefore proposed in [18], [19] to randomize the positions of the antenna elements, which was shown to reduce the resulting coherence significantly.

The combination of MIMO radar and CS was proposed in [20], [21] and was further studied in [22], [23] with emphasis on 1D MIMO arrays and DoA estimation. In particular, it was noted that a combination of MIMO processing and CS-based detection and DoA estimation is challenging, since the inherent structure of the resulting VAA entails high coherence values, similar to an ULAA. Randomizing the antenna element positions was shown to remedy this effect.

MIMO processing can readily be extended to 2D antenna arrays for 3D target localization and DoA estimation in azimuth and elevation [10], which is a pre-requisite with regard to future air traffic applications. DoA estimation for 2D MIMO arrays was considered in [24], where a sparse Bayesian learning based imaging algorithm was investigated, which addresses the aspect of off-grid targets. In the context of radar imaging, a genetic algorithm was used in [25] to reduce the mutual coherence of a 2D MIMO array. However, to the best of our knowledge, an optimization of 2D MIMO arrays by improving the degree of randomness – while additionally considering various restrictions regarding antenna element positioning – has not yet been addressed in the literature. Furthermore, in the previously mentioned publications [19]–[25] the investigations are limited to relatively large array sizes, whereas the influence of practicable 2D MIMO array sizes (e.g. for the use in airborne platforms) on CS performance and the resulting mutual coherence has not been addressed.

A. CONTRIBUTIONS AND OUTLINE

Motivated by the previous works outlined above, we investigate the combination of MIMO radar processing for 2D arrays with CS-based angular processing for 3D target localization and 2D DoA estimation in azimuth and elevation. In particular, we investigate in detail the benefits of randomized antenna element positions in one and two dimensions and devise optimized array geometries for practical aperture sizes. Novel aspects of our investigations are as follows:

- Regarding CS-based DoA estimation, we characterize the effect of improving the degree of randomness regarding antenna element positions on the resulting coherence of the CS measurement matrix. To the best of our knowledge, this has not yet been addressed for 2D MIMO arrays.
- While previous publications are limited to relatively large array sizes, we focus on 2D MIMO antenna arrays with practicable form factors fostering compact sensors for the use in airborne platforms and investigate the influence of small aperture sizes on the mutual coherence and on CS reconstruction.
- We propose different types of randomized 2D MIMO arrays and investigate the resulting performance differences with regard to CS-based DoA estimation using the Orthogonal Matching Pursuit (OMP) algorithm

[12, Ch.1], [14, Ch.3], [26]. Moreover, optimized array configurations are found for different side constraints, including practical limitations regarding the smallest realizable/ desired element spacing. Furthermore, area restrictions regarding antenna placement are considered to enable accommodation of additional components, thus fostering multi-functional sensors. Such compact, multi-functional MIMO radars might, for example, accommodate additional sensor elements within the aperture area of the MIMO array (e.g. a miniature optical or infrared camera) or additional hardware components for wireless communication applications [10], [27].

- When comparing the performance of MIMO arrays with conventional (randomized) antenna arrays, we distinguish between the number of *physical* and *virtual* antenna elements and demonstrate that the MIMO approach is clearly superior compared to fully randomized arrays, if the same number of *physical* antenna elements – and therefore similar hardware cost – is considered. On the other hand, the performance of fully randomized arrays with the same number of *virtual* antenna elements serves as an upper bound, which can be closely approached by our proposed randomized MIMO arrays.
- Based on the finding that the coherence of the measurement matrix is closely related to the maximum side-lobe level in the angular domain, which was shown in [18], [19] for conventional 1D arrays, we investigate the influence of a wide main lobe and the resulting low angular resolution on the CS DoA reconstruction performance, which is relevant for very compact form factors of the MIMO radar.

Extensive computer simulation results for different 3D target scenarios illustrate the advantages of our CS-based approach for multi-functional and compact MIMO radars using randomized antenna elements.

The remainder of this paper is organized as follows: In Section II, we derive the MIMO radar system model and extend it to describe a sparse target scenario. In Section III, the above mentioned novel aspects are addressed. In particular, we devise different types of randomized 2D MIMO arrays and investigate the influence of the corresponding random antenna configurations on the mutual coherence. In Section IV, corresponding numerical results are presented demonstrating the positive influence of improved antenna randomization on the reconstruction performance. Finally, conclusions are drawn in Section V, and interesting directions for future work are pointed out.

B. MATHEMATICAL NOTATION

Throughout this paper, vectors are represented in lower-case, bold-face and matrices in upper-case, bold-face fonts. For a vector $\mathbf{x}$, the i-th entry is denoted by $\mathbf{x}(i)$, while for a matrix $\mathbf{X}$ the (i, j)-th entry is described as $\mathbf{X}(i, j)$. $\mathbf{1}_N$ denotes a length-N row vector with unit entries. Furthermore, $(.)^*$ is the complex conjugate operator, $(.)^{\mathrm{T}}$ is the transpose operator and $(.)^{\mathrm{H}}$ denotes the complex conjugate-transpose operator. Additionally, $\|.\|_p$ represents the ℓ_p-norm, while $\|.\|_0$ is a pseudo-norm, which is defined as the number of non-zero elements of a matrix or vector. Finally, vec($\mathbf{X}$) describes a column-wise vectorization of a matrix $\mathbf{X}$.

II. SYSTEM MODEL

A. ASSUMPTIONS AND SIGNAL PROCESSING CONCEPT

Before deriving the system model in detail, we want to introduce the underlying assumptions concerning the air target scenario and the signal processing order.

- *Far field approximation*: It is assumed that the signal reflected from a target arrives as a planar wavefront at the radar antenna array. This assumption applies in general, if the distance r between the array and the target is larger than the Fraunhofer distance $d_{\mathrm{F}} = \frac{2D^2}{\lambda}$, with D being the aperture size of the antenna array and λ being the radar wavelength [28].
- *Point targets*: Throughout this contribution, it is assumed that all targets exhibit the characteristics of point targets. Correspondingly, targets are assumed to span a single angular sampling interval.
- *Clutter*: Clutter components caused by extended background structures (such as clouds) are not taken into account. Received radar signals are thus only corrupted by additive noise components.
- *Concept for radar signal processing*: It is assumed that all received signals are available in digitized form, i.e., each receive antenna element is equipped with a dedicated analog-/digital converter (ADC). Upon arrival of an echo signal at the radar receiver, analog signal processing is performed in the radar front-end. Afterwards, the received signal is Nyquist-sampled in the fast-time domain (representing the radial distance to a target) and in the slow-time domain (representing the radial velocity/ Doppler shift of a target after Fast-Fourier-Transform/ FFT-processing). Thus, the range-Doppler-matrix is obtained, which contains the received signal energy for each range-Doppler cell. At this point, a suitable detection algorithm may then be employed, in order to determine, in which range-Doppler cells a target is actually present. DoA estimation is then only performed for relevant range-Doppler cells containing target objects. Obviously, the chosen signal processing order fosters a sparse target scenario, since typical air scenarios contain only few targets and, after range compression and Doppler processing, point-like targets ideally appear as single samples in the range-/Doppler domain. Furthermore, it is rather unlikely that multiple targets are found within the same range-Doppler cell. Correspondingly, the number K of targets to be discriminated in the angular domain is usually either zero or one for a given range-Doppler cell. In the conventional processing scheme, DoA estimation is finally

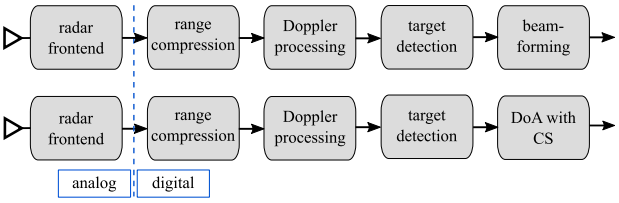

FIGURE 1. Schematic representation of the signal processing order for a radar utilizing DBF (top) or CS (bottom) in the angular domain.

performed by means of digital beamforming (DBF) and subsequent peak detection in the angular domain (Fig. 1, top). In the CS-based processing scheme, conventional DBF is replaced by a suitable CS-based algorithm (Fig. 1, bottom).

B. MIMO RADAR SYSTEM MODEL

In the first step, we consider a conventional, two-dimensional antenna array consisting of M transceivers distributed uniformly along two baselines in the xz-plane. The resulting geometrical model of the air target detection scenario is shown in Fig. 2. In this context, we define $\theta_{\mathrm{el}} = \phi_{\mathrm{az}} = 0°$ as boresight direction, where the elevation angle θ_{el} is defined as the angle between the xy-plane and the projection of the range vector $\mathbf{r}$ onto the yz-plane and the azimuth angle ϕ_{az} as the angle between the yz-plane and the projection of $\mathbf{r}$ onto the xy-plane. According to [29], the resulting 2D array factor (AF) is a multiplication of the azimuth pattern $\mathrm{AF}_{\mathrm{az}}$ with the elevation pattern $\mathrm{AF}_{\mathrm{el}}$. For M antennas with coordinates (x_m, z_m) and antenna weightings a_m, the AF can be written as

$$\mathrm{AF} = \mathrm{AF}_{\mathrm{az}} \cdot \mathrm{AF}_{\mathrm{el}} = \sum_{m=1}^{M} a_m \, e^{\mathrm{j}\frac{2\pi}{\lambda}[z_m \sin(\theta_{\mathrm{el}}) + x_m \sin(\phi_{\mathrm{az}})]}, \quad (1)$$

where $\lambda = \frac{c}{f_o}$ is the operating wavelength of the radar and c is the speed of light. In the next step, we expand the system model to a wideband MIMO radar array with M transmitters in z-direction and N receivers in x-direction. It is well known from the literature that if the M transmitted signals exhibit orthogonal characteristics, which for two signals $s_i(t)$ and $s_j(t)$ $(i \neq j)$ is defined as

$$\frac{1}{T}\int_0^T s_i(t) \cdot s_j^*(t)\, dt = 0 \quad (2)$$

for a suitable integration interval T, the individual contributions of M transmitting antenna elements can be separated at the receiver [8]–[11]. As a consequence, MN rather than $M + N$ received signals are available for joint spatial processing (which would be the case for a conventional antenna array with $M + N$ physical transceiver antenna elements). This not only results in a virtual enlargement of the physical antenna aperture, but also in an enhancement of the angular resolution. As an example, Fig. 3 shows an antenna array with $M = 4$ transmitting (Tx) and $N = 16$ receiving (Rx) antennas, resulting in a VAA with $MN = 64$ virtual elements, which can subsequently be utilized for DBF on receive – just as in the case of a physical array with $MN = 64$ elements. Signal orthogonality can, in principle, be realized in time domain, in frequency domain or in the signal domain, using orthogonal modulation schemes such as CDMA (code-division multiple access), OFDM (orthogonal frequency division multiplexing) or orthogonal codes [11]. Within the scope of this paper, we assume that ideal signal orthogonality is given. Consider a general MIMO antenna array with M transmitters and N receivers located on the baseline area in the xz-plane with coordinates (x_m, z_m) and (x_n, z_n), where $m = 1, \ldots, M$ and $n = 1, \ldots, N$. Furthermore consider a target scenario, where K targets are located in the same range-Doppler cell with distance r_k to the antenna array. The angular coordinates of the k-th target are given as (θ_k, ϕ_k) and its radar cross section (RCS) is denoted as σ_k. According to the geometrical model and the AF (1), the transmit and receive steering vectors for the k-th target can be described as

$$\mathbf{t}(k) = \left[e^{\mathrm{j}\zeta(1,k)} \quad \ldots \quad e^{\mathrm{j}\zeta(m,k)} \quad \ldots \quad e^{\mathrm{j}\zeta(M,k)}\right]^{\mathrm{T}} \quad (3)$$

$$\mathbf{r}(k) = \left[e^{\mathrm{j}\zeta(1,k)} \quad \ldots \quad e^{\mathrm{j}\zeta(n,k)} \quad \ldots \quad e^{\mathrm{j}\zeta(N,k)}\right]^{\mathrm{T}} \quad (4)$$

with

$$\zeta(m,k) = \frac{2\pi}{\lambda}[z_m \sin(\theta_k) + x_m \sin(\phi_k)] \quad (5)$$

$$\zeta(n,k) = \frac{2\pi}{\lambda}[z_n \sin(\theta_k) + x_n \sin(\phi_k)]\,. \quad (6)$$

Let $\mathbf{s}(t) = [s_1(t), \ldots, s_M(t)]^{\mathrm{T}}$ denote the vector consisting of M transmit signals. Then, after signal reflection by K targets, the received vector at the output of the N receive antenna elements can be expressed as [23]

$$\mathbf{d}(t) \propto \sum_{k=1}^{K} \mathbf{r}(k)\,\mathbf{t}^{\mathrm{T}}(k)\,\mathbf{s}\,(t - \tau_k)\;\sigma_k\,, \quad (7)$$

where $\tau_k = \frac{2r_k}{c}$ denotes the round trip delay associated with the k-th target. Since the antenna array has N physical Rx antennas, $\mathbf{d}(t) = [d_1(t), \ldots, d_N(t)]^{\mathrm{T}}$ consists of N measurements. In order to generate the VAA and thus MN virtual measurements, $\mathbf{d}(t)$ is cross-correlated with matched filters

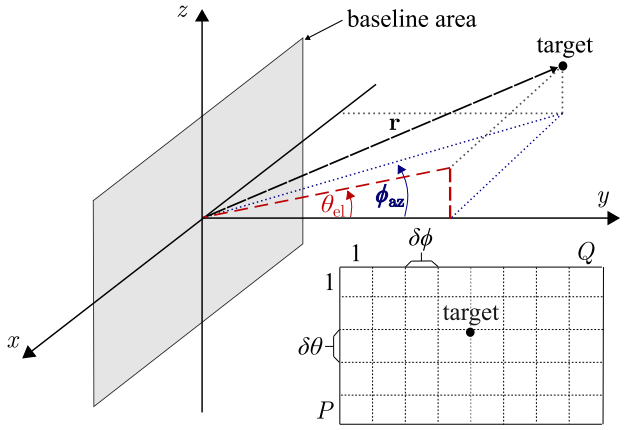

FIGURE 2. Geometrical model of the target detection scenario utilizing a two-dimensional antenna array.

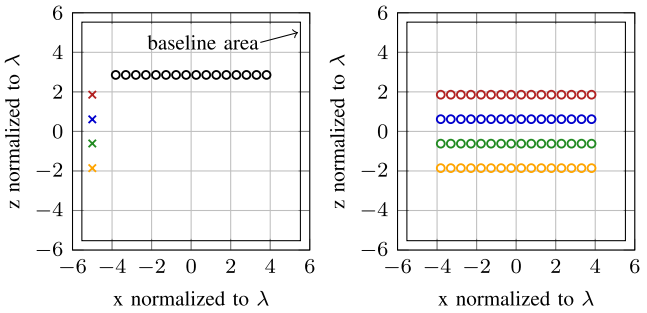

FIGURE 3. Example design of a 2D MIMO array with $M = 4$ Tx antennas (×), $N = 16$ Rx antennas (∘) (left) and the resulting VAA (right).

for every transmit signal $s_m(t)$. Because it is assumed that all transmit signals are mutually orthogonal, the resulting measurement vector $\mathbf{y}$ has the dimension $[MN \times 1]$ and can be described as [23]

$$\mathbf{y} = \text{vec}\left[\sum_{k=1}^{K} \mathbf{r}(k)\,\mathbf{t}^{\mathrm{T}}(k)\,\sigma_k \int \mathbf{s}\,(t-\tau_k)\,\mathbf{s}^{\mathrm{H}}\,(t-\tau_k)\,dt\right] \tag{8}$$

$$= \text{vec}\left[\sum_{k=1}^{K} \mathbf{r}(k)\,\mathbf{t}^{\mathrm{T}}(k)\,\sigma_k\right] \tag{9}$$

$$=: \mathbf{A}\,\boldsymbol{\sigma}\,. \tag{10}$$

$\mathbf{A}$ is an $[MN \times K]$ matrix with the (mn, k)-th element defined as

$$a_{mn,k} = e^{\mathrm{j}\frac{2\pi}{\lambda}[(z_m+z_n)\sin(\theta_k)+(x_m+x_n)\sin(\phi_k)]}, \tag{11}$$

and $\boldsymbol{\sigma}$ is a $[K \times 1]$ vector containing the RCS values of K targets.

C. COMPRESSIVE SENSING SYSTEM MODEL

Finally, we expand the derived MIMO radar system model (10) to describe a sparse target scenario, which is a key condition for CS reconstruction. To this end, we discretize the half-space in front of the MIMO antenna array to obtain a grid with Q grid points and uniform spacing $\delta\phi$ in azimuth and P grid points with uniform spacing $\delta\theta$ in elevation, see Fig. 2. This results in a structure with $Z = PQ$ grid points. For simplicity, it is assumed that potential targets are always located exactly on a grid point. For an unambiguous allocation of the grid points we define two dictionaries

$$\boldsymbol{\varphi} = \text{vec}\left(\mathbf{1}_P^{\mathrm{T}} \cdot \begin{bmatrix} 0 & \delta\phi & 2\delta\phi & \dots & (Q-1)\delta\phi \end{bmatrix}\right) \tag{12}$$

$$\boldsymbol{\vartheta} = \text{vec}\left(\begin{bmatrix} 0 \\ \delta\theta \\ 2\delta\theta \\ \vdots \\ (P-1)\delta\theta \end{bmatrix} \cdot \mathbf{1}_Q\right), \tag{13}$$

which consist of column- or row-wise repetitions of the corresponding grid spacings. The vectorization process, which generates two vectors $\boldsymbol{\varphi}$ and $\boldsymbol{\vartheta}$ with dimension $[Z \times 1]$, can be understood as an implementation of column wise sampling in angular domain. Introducing an auxiliary variable

$$\xi_i = [\boldsymbol{\varphi}(i)\ \boldsymbol{\vartheta}(i)] \tag{14}$$

with $i = 1 \dots Z$, a convenient and unique reference to Z angle pairs is then possible. According to (3) - (6) and (11) the steering vector for a target with angular position ξ_i can be described as

$$\boldsymbol{\psi}(\xi_i) = \begin{bmatrix} e^{\mathrm{j}\zeta(1,1,\xi_i)} & \dots & e^{\mathrm{j}\zeta(m,n,\xi_i)} & \dots & e^{\mathrm{j}\zeta(M,N,\xi_i)} \end{bmatrix}^{\mathrm{T}} \tag{15}$$

with

$$\zeta(m, n, \xi_i) := \frac{2\pi}{\lambda}[(z_m + z_n)\sin(\boldsymbol{\vartheta}(i)) + (x_m + x_n)\sin(\boldsymbol{\varphi}(i))]. \tag{16}$$

Since the target locations are generally unknown, steering vectors $\boldsymbol{\psi}(\xi_i)$ for all possible target positions ξ_i are generated and inserted column wise into a matrix

$$\boldsymbol{\Psi} = \begin{bmatrix} e^{\mathrm{j}\zeta(1,1,\xi_1)} & \dots & e^{\mathrm{j}\zeta(1,1,\xi_i)} & \dots & e^{\mathrm{j}\zeta(1,1,\xi_Z)} \\ \vdots & \dots & \vdots & \dots & \vdots \\ e^{\mathrm{j}\zeta(m,n,\xi_1)} & \dots & e^{\mathrm{j}\zeta(m,n,\xi_i)} & \dots & e^{\mathrm{j}\zeta(m,n,\xi_Z)} \\ \vdots & \dots & \vdots & \dots & \vdots \\ e^{\mathrm{j}\zeta(M,N,\xi_1)} & \dots & e^{\mathrm{j}\zeta(M,N,\xi_i)} & \dots & e^{\mathrm{j}\zeta(M,N,\xi_Z)} \end{bmatrix} \tag{17}$$

with dimension $[MN \times Z]$. In the context of CS, $\boldsymbol{\Psi}$ is denoted as sensing matrix in the sequel. As stated in Section II-A, it is very unlikely that multiple targets occupy the same range-Doppler cell. Therefore, within one range-Doppler cell, only $K \ll Z$ (and typically, $K = 0$ or $K = 1$) possible angular positions will actually contain targets, whereas $Z - K$ grid points remain empty (apart from noise, which is incorporated below). Let $\mathbf{X}$ denote a matrix with dimension $[P \times Q]$ that contains the RCS values for all Z grid points in the absence of noise. Correspondingly, $\mathbf{X}$ will consist of K non-zero and $Z - K$ zero entries. In other words, $\|\mathbf{X}\|_0 = K$ applies [14]. After vectorization, $\mathbf{X}$ is transformed into a K-sparse vector $\mathbf{x}$ with dimension $[Z \times 1]$ containing the RCS values for Z possible angular positions. Since we want to conduct CS-based DoA estimation, the goal is to reconstruct $\mathbf{x}$. For this purpose, we identify matrix $\mathbf{A}$ in (10) as the sensing matrix $\boldsymbol{\Psi}$ and $\boldsymbol{\sigma}$ as the K-sparse vector $\mathbf{x}$. Moreover, we add a vector $\mathbf{n}$ containing MN complex-valued, Gaussian distributed noise values, so as to capture the impact of ambient noise and receiver noise. The resulting matrix-vector equation

$$\underset{(MN\times 1)}{\mathbf{y}} = \underset{(MN\times Z)}{\boldsymbol{\Psi}} \cdot \underset{(Z\times 1)}{\mathbf{x}} + \underset{(MN\times 1)}{\mathbf{n}} \tag{18}$$

represents the fundamental CS equation, where $\mathbf{y}$ and $\boldsymbol{\Psi}$ are known and can be used to reconstruct the sparse vector $\mathbf{x}$.

III. INFLUENCE OF MIMO ANTENNA ARRAY DESIGN ON MUTUAL COHERENCE

The following section is divided into three parts. First, important conditions are introduced, which, if satisfied, guarantee reconstruction of a unique solution to (18). Next, as a new contribution, different 2D MIMO antenna array designs with increasing degree of randomness regarding antenna element positions are presented. In this context, special attention is paid to minimum antenna spacings as well as restricted areas for antenna placement. The latter is particularly attractive in order to foster a multi-functional sensor approach. In the last section, the influence of the array designs on mutual coherence is addressed. Here, as new contribution, arrays with practicable form factors are studied. In this context, it is found that the resulting wide main lobe of the antenna diagram has a significant influence on the resulting mutual coherence.

A. RECONSTRUCTION GUARANTEES

Since the main goal of compressed sensing is to reconstruct a sparse vector $\mathbf{x}$ from significantly less measurements (in our case MN) than the Nyquist rate suggests [12], [14], the resulting sensing matrix $\mathbf{\Psi}^{MN\times Z}$ consists of much fewer rows than columns ($MN \ll Z$). This property causes (18) to be underdetermined with infinitely many solutions. Nevertheless, under certain conditions (one of which being the *sparsity* of $\mathbf{x}$) it is possible to reconstruct a unique solution $\mathbf{x}$. A well-known sufficient condition is the *incoherence* of the sensing matrix $\mathbf{\Psi}$, which can be described by the mutual coherence $\mu(\mathbf{\Psi})$. It is defined as

$$\mu(\mathbf{\Psi}) = \max_{1\le i\neq j\le Z} \frac{|\langle \boldsymbol{\psi}_i^*, \boldsymbol{\psi}_j\rangle|}{\|\boldsymbol{\psi}_i\|_2 \, \|\boldsymbol{\psi}_j\|_2} \tag{19}$$

and determines the largest inner product between two ℓ_2-normalized column vectors $\boldsymbol{\psi}_i$ and $\boldsymbol{\psi}_j$ of the sensing matrix $\mathbf{\Psi}$. The mutual coherence $\mu(\mathbf{\Psi})$ is confined to the interval $\mu(\mathbf{\Psi}) \in \left[\sqrt{\frac{Z-MN}{MN(Z-1)}},\, 1\right]$ and reaches its maximum for two identical column vectors ($\boldsymbol{\psi}_i = \boldsymbol{\psi}_j$). The minimum is determined by the Welch bound [15]. Assuming that the mutual coherence is known, one can formalize the following condition on the sparsity of $\mathbf{x}$ for guaranteeing perfect reconstruction in the absence of noise [14], [15]:

$$\|\mathbf{x}\|_0 < \frac{1}{2}\left(1 + \frac{1}{\mu(\mathbf{\Psi})}\right). \tag{20}$$

Correspondingly, the mutual coherence $\mu(\mathbf{\Psi})$ should be as small as possible in order to perfectly reconstruct as many targets K as possible.

B. MIMO ANTENNA ARRAY DESIGN

It is well known from CS literature that independent identically distributed Gaussian or Bernoulli matrices are best suited for CS reconstruction [14], [15]. However, in our case the structure of the sensing matrix is determined by the antenna array geometry, which results in a deterministic sensing matrix $\mathbf{\Psi}$. In [18] and [19], the authors proposed to randomize the positions of the antenna elements, which was shown to reduce the resulting coherence significantly, thus improving the reconstruction rate. Before examining the influence of randomization on the mutual coherence, we first introduce a reference MIMO array, as shown in Fig. 3. It consists of $M = 4$ Tx antennas and $N = 16$ Rx antennas, which are located on a baseline area with a size of $11\,\lambda$ (0.25 m) in x-dimension. The antenna spacings amount to $d_x = 0.5\,\lambda$ and $d_z = 1.2\,\lambda$ in the considered example. The peculiarity of this layout is that the resulting VAA exhibits the properties of a filled array with $N = 64$ antennas, even though the physical antennas are placed exclusively at the edge of the aperture. This creates the possibility of filling the unused space with additional hardware components, such as optical sensors or wireless communication modules [10], [27]. In order to investigate, whether this advantage can possibly also be used in conjunction with CS-aided DoA, we start with the configuration "MIMO Array I" depicted in Fig. 4a, where the structure of the reference Array is only marginally modified. Compared to the other proposed antenna array designs, this layout therefore offers the largest possible installation space for additional hardware components (red dashed area). In the first step, the physical antennas are positioned at the maximum possible distance from each other (Tx antennas in z-direction, Rx antennas in x-direction). Next, a random shift is added in z-direction to the position of each transmitting antenna, while each receiving antenna is re-positioned by a random shift in x-direction. In this context, a constraint ensures that a pre-defined minimum antenna distance – in this example chosen as $\frac{\lambda}{2}$ – is not violated. One reason for maintaining a minimum antenna distance is to prevent mutual coupling effects. Another reason is that if antenna elements are separated by $\frac{\lambda}{2}$ or more, the rows of $\mathbf{\Psi}$ are approximately orthogonal. Thus, "each component of $\mathbf{y}$ captures *unique* information about $\mathbf{x}$" [19]. Fig. 4b shows an alternative configuration denoted "MIMO Array II" in the sequel, in which the Rx antennas are subject to an additional random shift in z-direction, while still leaving the maximum possible installation space for additional hardware components (red dashed area). A third MIMO antenna configuration is shown in Fig. 4c. The difference to the previous layout is that now the area between $-5.5\,\lambda$ and 0 in x-direction is made available for additional random shifts of the Tx antennas. By this means, additional degrees of freedom are gained with regard to virtual array formation, leading to improved reconstruction results, as will be seen in Sections III-C and IV. At the same time, a free installation area for multi-functional components (red dashed area) is preserved, although its size is reduced by 50 % compared to MIMO Array I and II. As a further result, after MIMO processing some antennas of the VAA may exceed the physical baseline area, thus potentially increasing the size of the virtual antenna aperture. By this approach, the aim of rather decreasing the additional sensor area than simply removing it, is to find out, whether a multi-functional sensor approach, as e.g. in [10], [27] can be combined with CS-aided DoA. As a

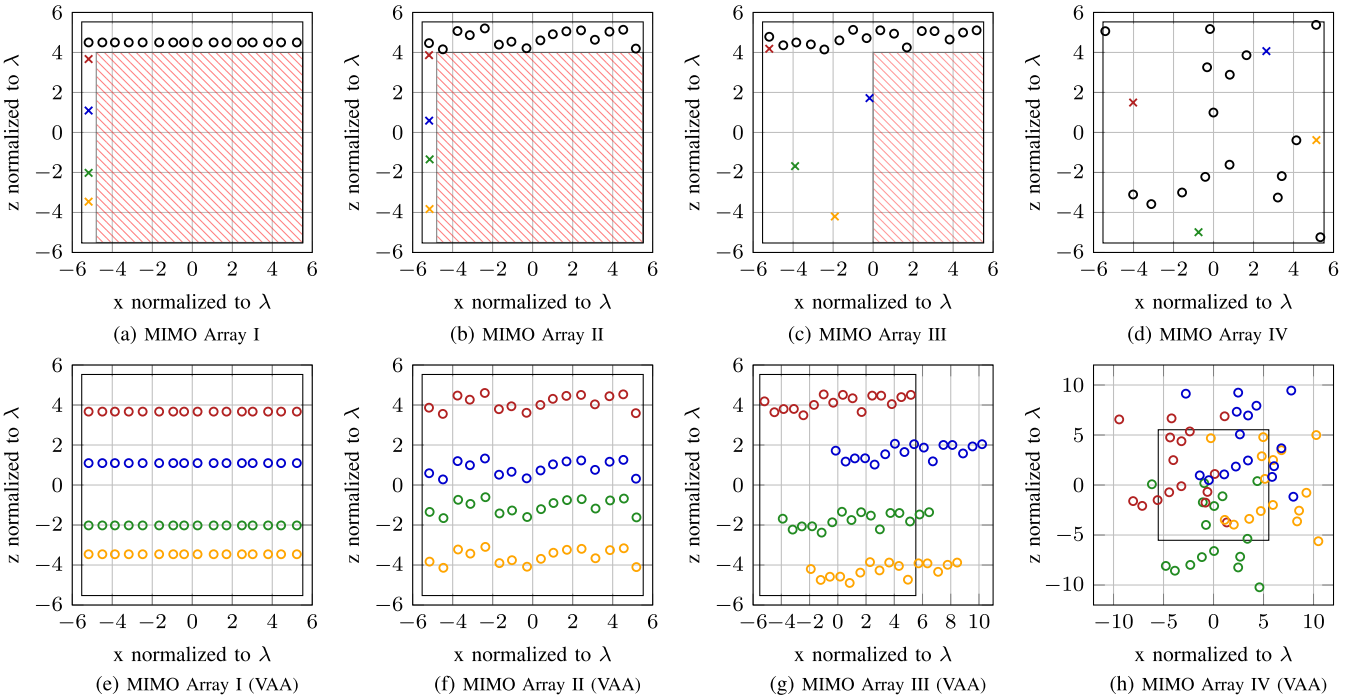

FIGURE 4. Designed MIMO antenna array configurations I-IV with $M = 4$ Tx antennas ($\times$) and $N = 16$ Rx antennas ($\circ$) (top) and the resulting VAA (bottom). The red dashed rectangle represents the restricted area for antenna element placement.

reference, we introduce the fourth configuration (Fig. 4d), where the free installation space is sacrificed completely in favor of further increased degrees of freedom regarding virtual array formation. In other words, "MIMO Array IV" employs the highest possible randomness regarding antenna element placement that can be achieved with MIMO signal processing. For this purpose, the Tx antennas are distributed in such a way that the subsequently added random shift in x- and z-direction is maximized, while the minimum distance of $\frac{\lambda}{2}$ is preserved. Afterwards, the Rx antennas are randomly distributed on the baseline without violating the minimum distance to one another and to the Tx antennas. In a final step, MIMO-processing is performed, resulting in a VAA that extends well beyond the physical baseline area. As a benchmark configuration, we finally define a fully random antenna array without MIMO signal processing, which will have the best properties with regard to a randomized sensing matrix.

To ensure a fair comparison, two configurations are considered, see Fig. 5. On the one hand, Random Array I consists of $N = 64$ randomly distributed Rx antennas, thus matching the number of $M \cdot N = 64$ *virtual* antennas of the configurations MIMO Array I - IV. On the other hand, Random Array II consists of $N = 20$ randomly distributed Rx antennas, which corresponds to the number of $M + N = 20$ *physical* antennas of the configurations MIMO Array I - IV. It is important to mention that both random array configurations are not limited by any restrictions (such as pre-defined minimum element distance), so as to capture characteristics of full randomization. The reason is that in [30] pure randomization

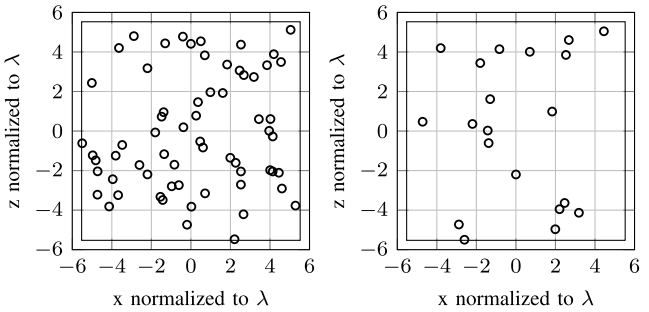

FIGURE 5. Random Array I with 64 Rx antennas (left), Random Array II with 20 Rx antennas ($\circ$) (right).

was shown to outperform other forms of conventional antenna randomization. Although pure randomization is unsuitable in practical applications, it serves primarily as a benchmark in this contribution. Note that Random Array II yields the fairest comparison with the different MIMO array configurations proposed above when it comes to hardware cost. Random Array I, on the other hand, gives an impression of what could be achieved if the number of virtual antenna elements of the proposed MIMO array configurations was distributed across the 2D physical baseline in an entirely random fashion.

C. INFLUENCE ON THE MUTUAL COHERENCE

In this section, the influence of the proposed antenna array configurations on the mutual coherence $\mu(\mathbf{\Psi})$ is examined with focus on practicable aperture sizes. For all subsequent investigations, the radar field of view is confined to the

interval $[-45°, 45°]$ in elevation and azimuth. Furthermore, a uniform grid spacing of 1° is assumed, if not stated otherwise. It is well known from radar literature that increasing the radar antenna aperture results in an enhanced angular resolution. This relation is commonly described by the dependence between the 3 dB-beamwidth of the main lobe $\Delta\phi_{3\text{dB}}$ and the radar antenna aperture D_x in azimuth and elevation D_z. For example, for a uniform 2D-array with uniform illumination across the antenna elements, this relation is given by [1, Ch. 13.2]:

$$\Delta\phi_{\text{az,3dB}} = \frac{50.8\,\lambda}{D_x}\,[°], \quad \Delta\phi_{\text{el,3dB}} = \frac{50.8\,\lambda}{D_z}\,[°]. \quad (21)$$

Moreover, in [19] an interesting relation between the antenna pattern of an array antenna and the mutual coherence $\mu(\boldsymbol{\Psi})$ of the resulting sensing matrix $\boldsymbol{\Psi}$ is reported. It was shown that the mutual coherence is a measure for the maximum side-lobe level (SLL). At this point, we want to further develop this relationship: The SLL may also include parts of the main lobe, if the lobe is relatively wide and extends over several spatial sampling points. Since the width of the main lobe in turn depends on the radar aperture, the mutual coherence is examined not only for the introduced antenna array configurations but also for different radar aperture sizes. On top of that, it is investigated, whether a wide main lobe has an influence on the mutual coherence. Because all configurations contain randomly generated antenna positions, the corresponding plots are obtained by calculating the arithmetic mean of 10^4 runs, in which only the antenna positions are re-allocated within each run. The resulting mutual coherence of the introduced antenna array configurations is illustrated in Fig. 6 by solid lines for a grid spacing of 1°. First of all, we note that up to a baseline area of $(0.25\,\text{m})^2$ all curves show a similar decreasing slope. However, for larger baseline areas the mutual coherence of MIMO Array I deteriorates significantly compared to the other array configurations. A possible cause for this is the high restriction on randomization of the antenna positions combined with the additional constraint that preserves a minimum antenna distance of $\frac{\lambda}{2}$. For baseline areas larger than $(0.5\,\text{m})^2$, first differences between the remaining antenna configurations become visible. It can be observed that the sensing matrix of Random Array II exhibits the highest coherence, followed closely by MIMO Array II. Contrary to expectations resulting from the challenge issued in [23], the sensing matrix of Random Array I does not always achieve lower coherence values than the other configurations. In fact, this only applies for baseline areas larger than $(0.75\,\text{m})^2$. For an area of $(0.5\,\text{m})^2$, the lowest coherence values are achieved by MIMO Array III and IV. At the end of this section it will be investigated whether this behavior is caused by the fact that the virtual aperture of MIMO Array III and IV is larger than the (physical) aperture of Random Array I (Fig. 4 & Fig. 5). When the baseline area is further increased to $(1\,\text{m})^2$, the curves start to flatten, making the differences between the configurations particularly clear. Now, Random

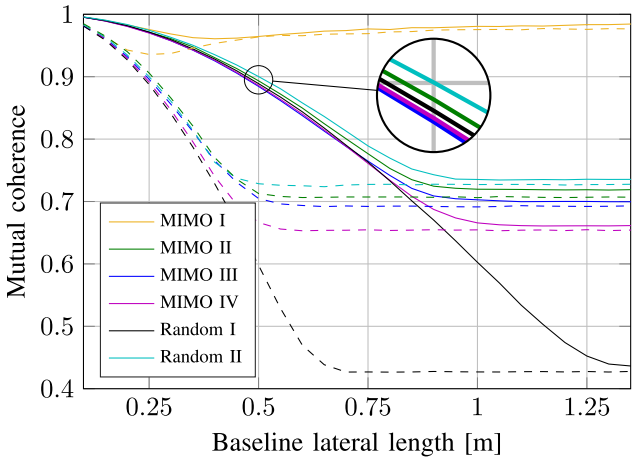

FIGURE 6. Mutual coherence $\mu(\Psi)$ of the sensing matrix Ψ for an increasing baseline area with a grid spacing of 1° (solid) and 2° (dashed).

Array I achieves the smallest coherence values, followed by MIMO Array IV, III, II and Random Array II. Despite considerable enlargement of the baseline area, MIMO Array I does not achieve coherence values below 0.95. Furthermore, for a baseline area larger than $(0.75\,\text{m})^2$, it can be observed that the slope of the MIMO array curves starts to decrease, until a further enlargement of the baseline area results in constant coherence values. Additional investigations have shown that the decrease of the slope can be shifted towards lower coherence values by employing more antennas.

From Fig. 4 & Fig. 5 it can be seen that the virtual aperture of MIMO Array III and IV is larger than the (physical) aperture of Random Array I. Consequently, the main lobe of MIMO Array III and IV is narrower compared to the main lobe of Random Array I. Since we have previously found that the SLL (which is related to $\mu(\boldsymbol{\Psi})$) may also include parts of the main lobe, we now investigate, whether a wide main lobe has an influence on the mutual coherence of the sensing matrix. Therefore $\mu(\boldsymbol{\Psi})$ is calculated for a grid spacing of 2°. Taking (21) into account with $D_x = D_z \approx 11\,\lambda$, it becomes clear that this adjustment excludes the main part of the main lobe from the calculation by causing neighboring grid points to be ignored. The results are shown in Fig. 6 with dashed lines. First of all, it can be seen that especially for small baseline areas the mutual coherence is significantly reduced for most antenna configurations. It can also be observed that, although the curves have a much steeper slope, they still approach the same constant value as in the 1° grid spacing case. Accordingly, an improvement is only achieved for small apertures, where the relative influence of the main lobe is the highest. Finally, it can be observed that Random Array I always achieves the smallest coherence values. In other words, if the influence of the main lobe is removed, also the advantage of the larger (virtual) aperture of MIMO Array III and IV over Random Array I is eliminated. Thus, the assumption made previously is confirmed. The relationship between the main lobe width and the mutual

coherence has not been investigated so far, because previously published papers ([19]–[25]) are limited to relatively large array sizes. This inherently prevents the generation of a wide main lobe, influencing the mutual coherence. In this section, it was shown that an enlargement of the baseline area and thus the radar aperture generally results in a smaller mutual coherence. Furthermore, considering MIMO Array I - IV, it was shown that an improvement of antenna randomization results in smaller coherence values. Regarding Random Array I and II, two observations are important to note. First of all, MIMO Arrays II - IV always generate lower coherence values than Random Array II. Second, Random Array I achieves the smallest coherence values, for a sufficiently large baseline area. Finally, it was shown that a wide main lobe, caused by a small radar aperture, has a significant impact on the mutual coherence of the sensing matrix.

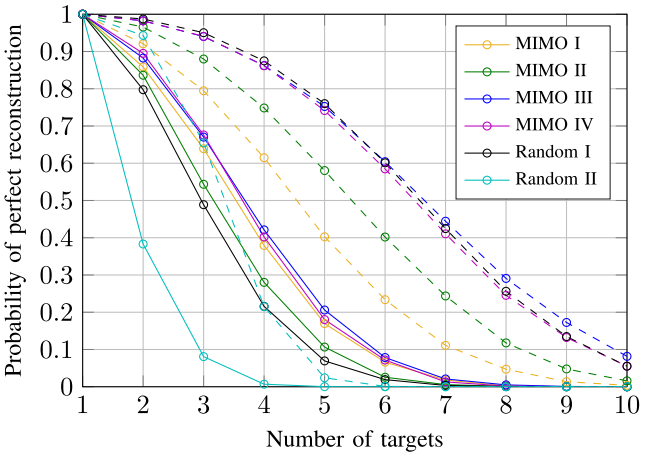

FIGURE 7. Number of perfectly reconstructible radar targets for a baseline area of $(0.25\,\mathrm{m})^2$ with an error tolerance of $\varepsilon = 0°$ (solid) and $\varepsilon = 1°$ (dashed).

IV. NUMERICAL RESULTS

After our initial comparisons based on mutual coherence, various performance aspects of the proposed MIMO array configurations are investigated in the sequel using results from extensive computer simulations.

A. NUMBER OF RECONSTRUCTIBLE TARGETS

It is known from the CS literature [12]–[15] that the mutual coherence $\mu(\boldsymbol{\Psi})$ of the sensing matrix $\boldsymbol{\Psi}$ determines how large the sparsity K may be, for the solution of (18) to be unique with high probability. Since in the previous section it was found that different configurations and increasing apertures have an influence on the mutual coherence, their impact on the number of reconstructible targets K will be studied in this section. To separate the influences from each other, the simulations are carried out without additive noise. Furthermore, it is important to note that a reconstruction is considered error-free only if all angular positions of the K targets have been estimated correctly. Contrary, a reconstruction is considered incorrect if at least one of K targets has been estimated incorrectly. In order to ensure reliable results, the curves are obtained by calculating the arithmetic mean of 10^5 runs, with random antenna positions and random target positions being regenerated within each run (along the lines of a Monte-Carlo simulation). Fig. 7 shows the results for a baseline area of $(0.25\mathrm{m})^2$. It can be seen that all configurations are able to reconstruct $K = 1$ target error-free (solid lines). This result can also be deduced from (20), since for $K = 1$ only $\mu(\boldsymbol{\Psi}) < 1$ must apply. This relation is fulfilled for all considered array configurations (cf. Fig. 6). Next, it can be seen that the majority of the curve progressions differ only slightly. This is due to the fact that for a baseline area of $(0.25\,\mathrm{m})^2$, all configurations generate an almost identical coherence value of $\mu(\boldsymbol{\Psi}) \approx 0.97$. One reason why Random Array II shows particularly poor reconstruction results could be that the configuration has an insufficient number MN of antennas to reconstruct more than one target without errors. This assumption is based on the sufficient condition

$$MN > 2K \ln\left(\frac{Z}{K}\right) \tag{22}$$

derived in [14] for large dimension random Gaussian matrices. Taking (22) as a rough reference, it is found that for a reliable reconstruction of $K = 2$ targets at least $MN = 34$ measurements are required. The fact that the number of measurements has an influence on the number of reconstructible targets is also supported by results from [19]. Finally, we note that Random Array I does *not* yield the best performance – in fact, all proposed MIMO arrays offer higher probability of perfect reconstruction, as soon as more than one target is supposed to be discriminated. In Section III-C, it was shown that a wide main lobe resulting from a small radar aperture has a significant negative impact on the mutual coherence. Besides, for conventional arrays it is well known that a wide main lobe leads to a low angular resolution and thus to inaccurate estimates of a target position. For this reason, subsequently the influence of a wide main lobe on CS DoA estimation is investigated. To this end, we allow an estimation error of $\varepsilon = 1°$, i.e., angular position estimates within $\pm 1°$ from the true target position are considered correct, which accounts for estimation inaccuracies caused by a wide main lobe. The results are displayed in Fig. 7 with dashed lines. As can be seen, the probability of reconstruction is increased significantly for all curves, when the requirements on the angular estimation accuracy are relaxed. Interestingly, the biggest improvement results for Random Array I, which now shows a similar reconstruction performance as MIMO Array III and IV. When the baseline area is increased to $(0.5\,\mathrm{m})^2$ (Fig. 8), it is found that except for MIMO Array I, all configurations show an improved reconstruction performance compared to Fig. 7, because the mutual coherence is reduced accordingly (cf. Fig. 6). In particular, MIMO Array IV and III show the best performance. They are able to reconstruct four targets with a probability of about 0.92,

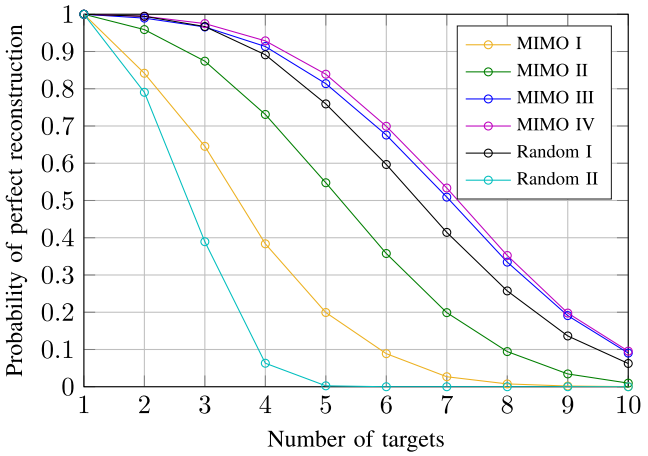

FIGURE 8. Number of perfectly reconstructible radar targets for a radar baseline area of $(0.5\,\mathrm{m})^2$ with an error tolerance of $\varepsilon = 0°$.

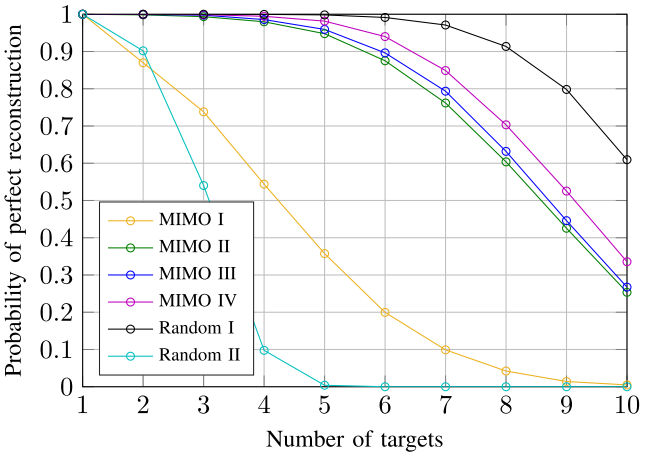

FIGURE 9. Number of perfectly reconstructible radar targets for a baseline area of $(1\,\mathrm{m})^2$ with an error tolerance of $\varepsilon = 0°$.

while Random Array I achieves a reconstruction probability of about 0.89, followed by MIMO Array II with a probability of about 0.75. This result can again be deduced from the coherence measurements in Fig. 6, as it shows an almost similar behavior. However, as before, the performance of Random Array II is worse than expected. Already for two targets the reconstruction probability drops below 0.8. Increasing the baseline area to $(1\,\mathrm{m})^2$, results in a significant improvement of the reconstruction performance of all configurations, except for MIMO Array I (Fig. 9). Now, as expected from Fig. 6, Random Array I shows the best reconstruction performance, followed by MIMO Array IV, III and II. Considering the configurations MIMO Array I - IV, it becomes particularly clear that an optimization of antenna randomization results in a better reconstruction performance. Interestingly, in most cases better results are obtained than predicted by (20), which for example indicates that to reconstruct $K = 2$ targets perfectly, a mutual coherence of $\mu(\mathbf{\Psi}) < \frac{1}{3}$ is required. Yet, none of the configurations reaches such low values, but still significantly more targets can be reconstructed without errors. In this context, the authors in [12] and [19] stated that results from the mutual coherence "are often overly pessimistic". Reexamining Fig. 7 – Fig. 9, one will notice that the performance difference between MIMO Array III and MIMO Array IV is rather marginal, whereas the difference to MIMO Array II and especially MIMO Array I is much more significant. Accordingly, maximal randomization as in MIMO Array IV, while sacrificing the free installation space, does not provide a significant advantage. On the other hand, allocating the largest possible installation space leads to a strong degradation of reconstruction performance. Therefore, it seems that MIMO Array III offers the best compromise for a multi-functional sensor approach that performs CS-aided DoA. Moreover, if integrated patch antenna elements are supposed to be employed, routing will be much simplified compared to MIMO Array IV, since in MIMO Array III antenna elements are not randomly distributed across the entire physical aperture area. Thus, they can be connected relatively easily via the upper and the left edge of the physical aperture, which enables a simplified fabrication process.

In this section, it was shown that increasing the baseline area and improving antenna randomization both have a positive effect on the number of reconstructible targets. On top of that, it was shown that antenna array configurations with MIMO processing outperform pure random configurations, if the number of antenna elements in the random array corresponds to the number of *physical* antenna elements in the MIMO array.

B. RECONSTRUCTION WITH ADDITIVE NOISE AND ARRAY OPTIMIZATION

In this section, the influence of improved antenna randomization on the reconstruction in the presence of additive white Gaussian noise (AWGN) is investigated. Since the signal processing order mentioned in Section II-A fosters a sparse air target scenario, where usually $K \leq 1$ targets are present within a given range-Doppler cell, the subsequent investigations are carried out for a scenario with $K = 1$ target. Instead of simply averaging the curves from 10^5 different, randomly generated array configurations as in the previous section, an exhaustive search was conducted for every antenna configuration and for the baseline areas $(0.25\,\mathrm{m})^2$, $(0.5\,\mathrm{m})^2$ and $(1\,\mathrm{m})^2$ in order to find an antenna arrangement in each case, which offers improved performance in reconstruction with additive noise. Fig. 4a-5 show the optimized antenna arrays for a baseline area of $(0.25\,\mathrm{m})^2$. Comparisons with averaged curves have shown that for a given error probability of 10^{-4} the required signal-to-noise ratio (SNR) was reduced by 3 dB for $(0.25\,\mathrm{m})^2$, 2 dB for $(0.5\,\mathrm{m})^2$ and 0.5 dB for $(1\,\mathrm{m})^2$ apertures on average. As in the previous section, the curves are obtained by calculating the arithmetic mean of 10^5 runs. However, now the optimized, random antenna positions are fixed and only the random target positions and the random noise vectors were generated within each simulation run.

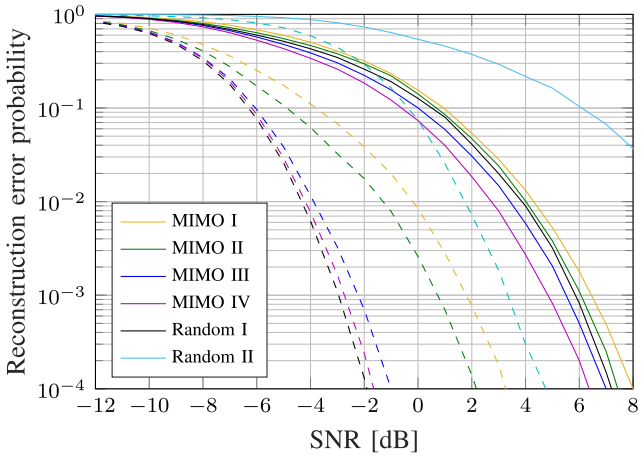

FIGURE 10. Reconstruction error probability for $K = 1$ target at a baseline area of $(0.25\,\mathrm{m})^2$ with an error tolerance of $\varepsilon = 0°$ (solid) and $\varepsilon = 1°$ (dashed).

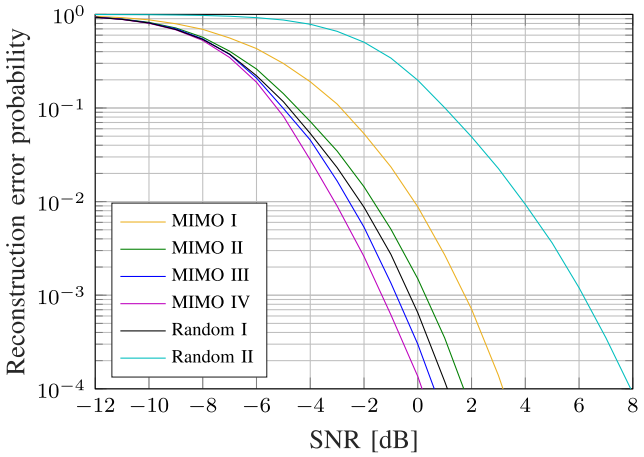

FIGURE 11. Reconstruction error probability for $K = 1$ target at a baseline area of $(0.5\,\mathrm{m})^2$ with an error tolerance of $\varepsilon = 0°$.

Fig. 10 shows the results for a baseline area of $(0.25\mathrm{m})^2$. First of all, it can be seen that Random Array II requires a significantly higher SNR of up to 6 dB to achieve the same error probability as MIMO Array I and II. As in the previous investigations, MIMO Array IV and III show the best reconstruction performance for a baseline area of $(0.25\mathrm{m})^2$. For example, at an SNR of 6 dB, the error probability of MIMO Array IV is almost a decade smaller compared to that of MIMO Array I. However, as in the previous section, the performance of Random Array I is worse than MIMO Array III and IV. This result is examined in the following by allowing an error of $\varepsilon = 1°$ regarding target reconstruction in order to account for estimation inaccuracies caused by a wide main lobe associated with the small aperture size. The corresponding results are shown in Fig. 10 by dashed lines. It can be seen that a 1° error tolerance leads to significantly better reconstruction results for all array configurations. For a given error probability of 10^{-4}, an SNR improvement of up to 8 dB can be observed. Consequently, it becomes obvious that the main reconstruction error source for a small baseline area, e.g. $(0.25\,\mathrm{m})^2$, is the low angular resolution resulting from a wide main lobe. Furthermore, it can be observed that Random Array I exhibits the best reconstruction performance closely followed by MIMO Array IV and III. Generally, MIMO Array III and IV have a significant advantage over Random Array I, since they achieve larger (virtual) apertures. This inherently decreases the main lobe width, thus mitigating the main source for estimation inaccuracies. However, if an angular estimation error of $\varepsilon = 1°$ is allowed, the main error source of Random Array I is basically excluded. Consequently, the advantage of MIMO Array III and IV over Random Array I disappears. It is important to mention that this advantage is only noticeable for small baseline areas, where the impact of a wide main lobe is most significant. When the baseline area is increased to $(0.5\,\mathrm{m})^2$ (Fig. 11), it is generally found that the reconstruction performance of all configurations is significantly improved compared to Fig. 10. Still, in accordance with the results presented in Section IV-A, Random Array II showed by far the poorest reconstruction results, whereas MIMO Array IV and III showed the best reconstruction performance, followed by Random Array I. To achieve an error probability of 10^{-4}, Random Array II required an SNR of 8 dB, MIMO Array I required an SNR of 3 dB and MIMO Array II required an SNR of 1.8 dB. Random Array I required an SNR of at least 0.5 dB, followed by MIMO Array III with an SNR of 0.3 dB and MIMO Array IV with an SNR of 0 dB. Comparing the error probabilities of the MIMO Arrays at 0 dB SNR, we found that the error probability of MIMO Array IV was more than one decade smaller than that of MIMO Array II and almost two decades smaller than that of MIMO Array I. Accordingly, it can be concluded that improving the randomization of antenna elements results in a significant improvement of the reconstruction performance. When the baseline area is further increased to $(1\,\mathrm{m})^2$, the reconstruction performance of all configurations, except for MIMO Array I, is further improved (Fig. 12). As in the previous case, Random Array II shows the worst reconstruction performance, even though for a given error probability the SNR improvement is up to 4 dB compared to a baseline area of $(0.5\,\mathrm{m})^2$. Now, as expected from the results in Section IV-A, Random Array I achieves the best reconstruction performance, closely followed by MIMO Array IV and III, which show only slightly inferior results. As in the previous section, when re-examining Fig. 10 – Fig. 12, it can be observed that the performance difference between MIMO Array III and MIMO Array IV is relatively small, whereas the difference to MIMO Array II and especially to MIMO Array I is much more significant. Due to the fact that MIMO Array III offers good reconstruction performance while still leaving a relatively large fraction of free installation space for additional sensors, it is therefore well suited for a multi-functional sensor approach performing CS-aided DoA. In this section, it was shown that improving the antenna randomization as well as increasing the radar aperture have

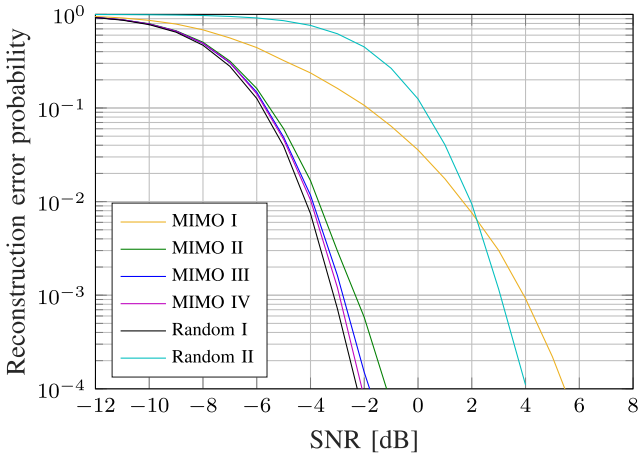

FIGURE 12. Reconstruction error probability for $K = 1$ target at a baseline area of $(1\,\mathrm{m})^2$ with an error tolerance of $\varepsilon = 0°$.

a significant impact on the CS reconstruction performance in the presence of noise. It was found that by improving the antenna randomization the resulting error probability can be reduced by up to two decades. Furthermore, it was found that by increasing the baseline area from $(0.25\,\mathrm{m})^2$ to $(1\,\mathrm{m})^2$ the SNR, which is required for a specific error probability could be reduced by 8 dB for some antenna configurations.

V. CONCLUSION

We have investigated the problem of DoA estimation for air targets using a compact MIMO radar sensor in combination with CS techniques, so as to enhance the angular resolution while at the same time exploiting the sparseness of typical air scenarios. To this end, we have proposed and optimized different types of MIMO antenna arrays with increasing degrees of randomness regarding the positioning of antenna elements, while taking practical constraints into account concerning a pre-defined minimum antenna element spacing as well as reserved areas within the overall antenna aperture for additional sensor or wireless communication modules, to enable a multi-functional design. We investigated the performance of the proposed MIMO array configurations with regard to the mutual coherence of the resulting sensing matrix, the number of simultaneously detectable targets in the absence of noise, and the reconstruction error probability in the presence of a single target in AWGN. It was shown that an increased degree of randomness consistently improves the performance of our MIMO arrays, which is in line with common findings from CS theory advocating random sensing matrices. Moreover, increasing the physical size of the array baseline also offers performance improvements, when the grid size in angular domain is fixed, which is similar to conventional digital beamforming. Interestingly, our proposed MIMO Arrays II-IV significantly outperform fully random arrays with the same number $(M + N)$ of *physical* antenna elements at comparable hardware cost. Moreover, MIMO Array III and IV even offer a performance typically close to a fully random array employing MN antenna elements, which corresponds to the number of *virtual* antenna elements in the MIMO arrays (and would therefore entail considerably higher hardware costs for the random array). Although the reserved installation space within the physical baseline area of MIMO Array III has been reduced, it could still be used for accommodating an additional sensor or a wireless communication module. This feature was dropped for MIMO Array IV in favor of an increased degree of randomness. Yet, the additional performance gain of MIMO Array IV compared to MIMO Array III was usually rather small, so that MIMO Array III seems to be a practicable configuration, if a compact multi-functional sensor is desired. Furthermore, we investigated the impact of a wide main lobe on the mutual coherence, caused by small aperture sizes typical for airborne applications. In particular, it was found that fundamental limits regarding angular estimation accuracy, which are well-known from conventional arrays, also apply for our CS reconstruction results obtained with the randomized MIMO arrays. Therefore, similar to conventional arrays, suitable tolerance intervals regarding angular estimates need to be accepted also in this case, in order to account for the impact of a relatively wide main lobe.

For future work, it will be interesting to investigate alternative CS techniques in addition to the OMP algorithm considered within the scope of this paper. By this means, the detection performance of the MIMO arrays might be further improved. Moreover, off-grid effects have not been considered so far, and corresponding investigations will be subject for future work. Of particular interest it will be to perform similar MIMO array optimization steps, in order to learn the benefits of increased degrees of randomness under practical array design constraints. Another interesting aspect for future investigations is the application of optimization algorithms that might further improve random positioning of antenna elements, taking into account the reserved areas for multi-functional sensors.

REFERENCES

[1] M. Skolnik, *Radar Handbook*, 3rd ed. New York, NY, USA: McGraw-Hill, 2008.
[2] M. A. Richards, J. A. Scheer, and W. A. Holm, *Principles of Modern Radar*, vol. 1. Rijeka, Croatia: SciTech, 2010.
[3] W. L. Melvin and J. A. Scheer, *Principles of Modern Radar*, vol. 2. Rijeka, Croatia: SciTech, 2013.
[4] J. A. Scheer and W. L. Melvin, *Principles of Modern Radar*, vol. 3. Rijeka, Croatia: SciTech, 2013.
[5] C. V. Jackowatz, *Spotlight Mode Synthetic Aperture Radar: A Signal Processing Approach*. New York, NY, USA: Springer, 1996.
[6] I. G. Cumming and F. H. Wong, *Digital Processing of Synthetic Aperture Radar Data: Algorithms and Implementation*. Norwood, MA, USA: Artech House, 2005.
[7] M. Kirscht, J. Mietzner, B. Bickert, A. Dallinger, J. Hippler, J. Meyer-Hilberg, R. Zahn, and J. Boukamp, "An airborne radar sensor for maritime and ground surveillance and Reconnaissance—Algorithmic issues and exemplary results," *IEEE J. Sel. Topics Appl. Earth Observ. Remote Sens.*, vol. 9, no. 3, pp. 971–979, Mar. 2016.
[8] J. Li and P. Stoica, *MIMO Radar Signal Processing*. Hoboken, NJ, USA: Wiley, 2008.
[9] A. Haimovich, R. Blum, and L. Cimini, "MIMO radar with widely separated antennas," *IEEE Signal Process. Mag.*, vol. 25, no. 1, pp. 116–129, Jan. 2008.

[10] E. Miralles, T. Multerer, A. Ganis, B. Schoenlinner, U. Prechtel, A. Meusling, J. Mietzner, C. Weckerle, H. Esteban, M. Vossiek, M. Loghik, and V. Ziegler, "Multifunctional and compact 3D FMCW MIMO radar system with rectangular array for medium-range applications," *IEEE Aerosp. Electron. Syst. Mag.*, vol. 33, no. 4, pp. 46–54, Apr. 2018.
[11] A. Santra, A. Ganis, J. Mietzner, and V. Ziegler, "Ambiguity function and imaging performance of coded FMCW waveforms with fast 4D receiver processing in MIMO radar," *Digit. Signal Process.*, vol. 97, p. 13, Feb. 2020.
[12] M. A. Davenport, M. F. Duarte, Y. C. Eldar, and G. Kutynio, *Introduction to Compressed Sensing*. Cambridge, U.K.: Cambridge Univ. Press, 2012.
[13] Y. C. Eldar and G. Kutyniok, *Compressed Sensing: Theory Applications*. Cambridge, U.K.: Cambridge Univ. Press, 2012.
[14] S. Foucart and H. Rahut, *A Mathematical Introduction to Compressive Sensing*. New York, NY, USA: Springer, 2013.
[15] G. Kutyniok, "Compressed sensing," *DMV Mitteilungen*, vol. 22, pp. 24–29, Mar. 2014.
[16] M. A. Herman and T. Strohmer, "High-resolution radar via compressed sensing," *IEEE Trans. Signal Process.*, vol. 57, no. 6, pp. 2275–2284, Jun. 2009.
[17] J. H. G. Ender, "On compressive sensing applied to radar," *Signal Process.*, vol. 90, no. 5, pp. 1402–1414, May 2010.
[18] L. Carin, "On the relationship between compressive sensing and random sensor arrays," *IEEE Antennas Propag. Mag.*, vol. 51, no. 5, pp. 72–81, Oct. 2009.
[19] L. Carin, D. Liu, and B. Guo, "Coherence, compressive sensing, and random sensor arrays," *IEEE Antennas Propag. Mag.*, vol. 53, no. 4, pp. 28–39, Aug. 2011.
[20] C.-Y. Chen and P. P. Vaidyanathan, "Compressed sensing in MIMO radar," in *Proc. 42nd Asilomar Conf. Signals, Syst. Comput.*, Oct. 2008, pp. 41–44.
[21] Y. Yu, A. P. Petropulu, and H. V. Poor, "MIMO radar using compressive sampling," *IEEE J. Sel. Topics Signal Process.*, vol. 4, no. 1, pp. 146–163, Feb. 2010.
[22] M. Rossi, A. M. Haimovich, and Y. C. Eldar, "Spatial compressive sensing in MIMO radar with random arrays," in *Proc. 46th Annu. Conf. Inf. Sci. Syst. (CISS)*, Mar. 2012, pp. 1–6.
[23] M. Rossi, A. M. Haimovich, and Y. C. Eldar, "Spatial compressive sensing for MIMO radar," *IEEE Trans. Signal Process.*, vol. 62, no. 2, pp. 419–430, Jan. 2014.
[24] Z. Jiao, C. Ding, X. Liang, L. Chen, and F. Zhang, "Sparse Bayesian learning based three-dimensional imaging algorithm for off-grid air targets in MIMO radar array," *Remote Sens.*, vol. 10, no. 3, p. 369, Feb. 2018.
[25] C. Dai, L. Zhou, X. Liang, and Y. Wu, "Optimal MIMO array for compressive sensing image formation," *J. Electromagn. Waves Appl.*, vol. 28, no. 16, pp. 2049–2058, Oct. 2014.
[26] T. T. Cai and L. Wang, "Orthogonal matching pursuit for sparse signal recovery with noise," *IEEE Trans. Inf. Theory*, vol. 57, no. 7, pp. 4680–4688, Jul. 2011.
[27] J. Mietzner, S. Lutz, C. Weckerle, B. Hofstaetter, E. Miralles, A. Ganis, T. Multerer, J. Puchinger, U. Prechtel, V. Ziegler, and A. Meusling, "Compact 3D MIMO radar—Antenna array design and experimental results," in *Proc. Eur. Radar Conf. (EURAD)*, Oct. 2017, pp. 130–133.
[28] Z. Chen and G. Goreka, *Introduction to Direction-of-Arrival Estimation*. Norwood, MA, USA: Artech House, 2010.
[29] C. A. Balanis, *Antenna Theory*, 3rd ed. Hoboken, NJ, USA: Wiley, 2005.
[30] I. Stojanovic, M. Cetin, and W. C. Karl, "Compressed sensing of monostatic and multistatic SAR," *IEEE Geosci. Remote Sens. Lett.*, vol. 10, no. 6, pp. 1444–1448, Nov. 2013.

ANDREJ HARLAKIN received the M.Sc. degree in electrical engineering and business administration from Kiel University, Germany, in 2019, where he is currently pursuing the Ph.D. degree with the Faculty of Engineering. Since 2019, he has been a Research and Teaching Assistant with the Chair of Information and Coding Theory, Kiel University. His current research interests include underwater optical wireless communications, localization, and radar signal processing.

JAN MIETZNER (Senior Member, IEEE) received the Ph.D. degree (Hons.) in electrical and information engineering from Christian-Albrechts University (CAU), Kiel, Germany, in 2006.

In 2000, he spent six months with the Global Wireless Systems Research Group, Bell Laboratories, Lucent Technologies, Swindon, U.K., working on software solutions for the EDGE mobile radio system. From 2007 to 2008, he was a Postdoctoral Research Fellow with The University of British Columbia, Vancouver, BC, Canada, sponsored by the German Academic Exchange Service (DAAD), where he worked on algorithms for relay-assisted ultra-wideband and cognitive-radio systems. In 2009, he joined Airbus DS (now Hensoldt), Ulm, Germany, where he worked in the areas of jamming and radar systems and was the Technical Project Manager of multiple-input multiple-output (MIMO) radar development. In September 2017, he became a Professor of communications engineering with the Hamburg University of Applied Sciences (HAW). His research interests include theoretical and practical aspects of communication and radar systems. He has published more than 20 journal articles and 40 conference papers. He was a co-recipient of the 2010 Best Paper Award from the German Information Technology Society (VDE/ITG). He has served as a Technical Program Committee Member for various IEEE conferences and was the Track Co-Chair of VTC-Fall 2014. He serves as an Editor for the IEEE Wireless Communications Letters.

PETER ADAM HOEHER (Fellow, IEEE) received the M.Sc. degree in electrical engineering from RWTH Aachen University, Aachen, Germany, in 1986, and the Ph.D. degree in electrical engineering from the University of Kaiserslautern, Kaiserslautern, Germany, in 1990. From 1986 to 1998, he was with the German Aerospace Center (DLR), Oberpfaffenhofen, Germany. From 1991 to 1992, he was on leave at AT&T Bell Laboratories, Murray Hill, NJ. Since 1998, he has been a Full Professor of electrical and information engineering with Kiel University, Kiel, Germany. His research interests include wireless communications and applied information theory. Since 2014, he has been a Fellow of the IEEE for contributions to decoding and detection that include reliability information.

ASKOLD MEUSLING received the Diploma and Ph.D. degrees in electronics from Otto-von-Guericke University Magdeburg, Magdeburg, Germany. He was an ASIC Designer of mainframe processors and the Manager position of innovation management with Siemens for ten years. He was an Architect and the Project Leader of enterprise software projects with Accenture for three years. Since 2004, he has been the Department Lead, where he was responsible for the development of radio reconnaissance and communication jamming system. Within the central research department of Airbus, he promotes the development of multiple-input multiple-output radar technology for several applications. He is an Inventor or a Co-Inventor of eight patents and has coauthored several conference papers and publications.